

Flow Interaction Between Porous and Non-porous region in a Channel Partially Filled with a Porous Block: Pore-scale LES Study

Mohammad Jadidi¹, Yasser Mahmoudi²

Department of Mechanical, Aerospace and Civil Engineering (MACE), University of Manchester, M13 9PL, UK
¹mohammad.jadidi@manchester.ac.uk
²yasser.mahmoudi@manchester.ac.uk

Abstract – The present study investigates fluid flow interaction between porous and non-porous regions in a channel partially filled with a porous block. For this purpose, a detailed pore-scale large eddy simulation is utilized. Flow visualization shows that some portion of the fluid entering the porous blocks is pushed upwards to the porous-fluid interface and leaves the porous region; this phenomenon is called flow leakage. Spectral analysis of vertical velocity and correlation coefficients confirm the flow leakage. Below the porous interface, the magnitude of correlation coefficients exposes a strong positive correlation between vertical velocity fluctuations that reveals the upward tendency of flow in the porous region. This trend is also observed across the porous interface which confirms momentum transfer through the porous interface. Moreover, spectral analysis of vertical velocity reveals that the dominant frequencies within the porous region exist in the non-porous region where the flow leakage is pronounced. This observation shows strong momentum transfer between the porous and non-porous regions due to the flow leakage.

Keywords: Porous flow; Flow leakage; Large eddy simulation (LES); spectral analysis; correlation coefficient.

1. Introduction

Partial blockage of the flow area in a composite porous-fluid system subdivides the turbulent flow into two different flow regions separated by a permeable interface (Fig. 1). The first is the non-porous region (surface or free) flow, which overlies the interface. The second is the porous region (sub-surface or pore) flow, which happens within the porous block. Momentum transport across the interface between the porous and non-porous region adds several complex physics to the problem where flow interactions between the free flow and the pore flow take place. This phenomenon introduces several open questions regarding the links between the sub-surface and surface flow that is gaining expanding academic and industrial attention [1-5].

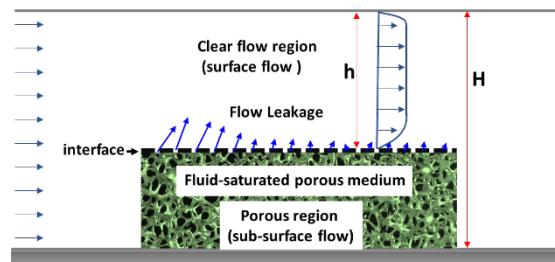


Fig. 1 A composite porous-fluid system showing flow leakage from the interface

Latest findings have shown that the interplay between the porous and non-porous flow may cause the flow in the porous region to leave it halfway through to the clear region before it reaches the end of the porous media: flow leakage [6]. The flow leakage can alter the flow features at the interface and hence affect the exchange of mean and turbulent properties between the clear and porous regions. For instance, the fluid dynamics of a channel partially filled with a metal foam block have been studied by Shikh Anuar, et al. [7]. They showed that for low-pore density foam, fluid is permitted to pass freely through the porous structure, while higher-pore density foam imposes more restrictions on the flow, pushing the fluid away from the foam into the non-porous region at the top of the foam block, before reaching the foam end. Recently a similar flow behaviour in a composite porous-fluid system was reported by Jadidi, et al. [8] using a pore-scale LES. They showed that

the flow leakage leads to the formation of counter-rotating vortex pairs of the flow within and above the porous region and alters the coherent structures above the interface. They also argued that the magnitude of the turbulent kinetic energy in porous cases is decreased drastically above the interface compared to the solid case.

Despite growing attention to the flows in a channel partially filled with porous block, the interactions between porous and non-porous flow have not been sufficiently documented and the mechanism of turbulence transportation across the interface is still not fully understood. Tackling this problem requires an in-depth understanding of the fluid flow in composite porous-fluid systems at the pore level. The issue of this study is to explore the flow interaction between the porous and non-porous regions across the interface in both spatial and spectral domains. For this purpose, a channel partially filled with a porous block is investigated using detailed pore-scale large eddy simulations (LES). The phenomena of flow leakage from the porous region into the non-porous region through the porous-fluid interface is explained and its effects on the momentum transfer are analysed. Findings can be utilized to support interface models at the macroscopic scale in which the interface is modelled by a surface of discontinuity that divides the domain into two homogeneous regions: a porous and a non-porous region [9, 10].

2. Computational Domain And Boundary Conditions

The computational domain is a channel partially filled with two different porous blocks and a solid block depicted in Fig. 2. The first porous block is formed from a rectangular cross-section ligament with a thickness of $0.52D$. The blockage ratio (i.e., ratio of the height of the porous region to the channel height) is 0.5. The flow Reynolds number based on the channel height and inlet velocity is 3600. Fig. 2(b) shows two spanwise and streamwise locations where LES results are presented and discussed, namely: “trough plane” and “crest plane”. The interface on the crest plane is locally impermeable, allowing no flow penetration at this location. Nonetheless, the trough plane has a fully open (permeable) interface, which enables fluid exchange between the porous and non-porous regions.

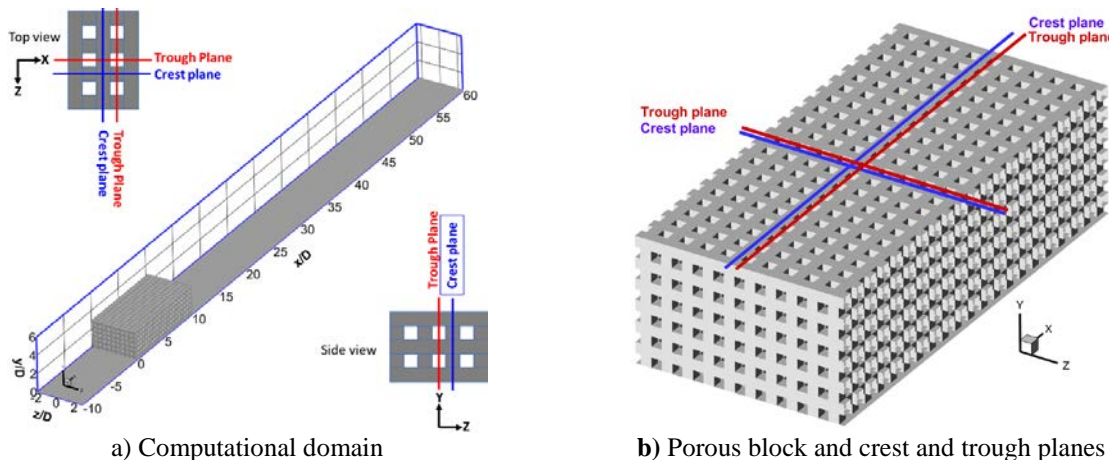


Fig. 2 Computational domain; a) Porous block formed from rectangular cross-section ($0.52D \times 0.52D$) ligament with porosity $\Phi = 48\%$ and permeability $K = 2.85 \times 10^{-8} m^2$. Illustration of two spanwise and streamwise locations for presenting results, the red line lies over the “trough plane” and the blue line lies over the “crest plane”

3. Numerical Methods

3.1. Governing equations and sub-grid scale modelling

By applying top hat filter to the governing equations of the flow field, the incompressible LES filtered equations for the resolved fields are derived as follows [11]:

$$\frac{\partial \bar{u}_i}{\partial x_i} = 0 \quad (1)$$

$$\frac{\partial \bar{u}_i}{\partial t} + \frac{\partial}{\partial x_j} (\bar{u}_i \bar{u}_j) = -\frac{1}{\rho} \frac{\partial \bar{p}}{\partial x_i} + \frac{\partial}{\partial x_j} \left(\nu \frac{\partial \bar{u}_i}{\partial x_j} - \tau_{ij} \right) \quad (2)$$

where, \bar{u}_i and \bar{p} are the filtered velocity in i^{th} direction and pressure, respectively. These equations govern the evolution of the large, energy-carrying scales of motion. The effect of the small scales appears in the flow field utilizing sub-grid scale (SGS) turbulent stress tensor, τ_{ij} , which is unknown and must be modelled.

$$\tau_{ij} - \frac{1}{3} \tau_{kk} \delta_{ij} = -2\nu_{SGS} \bar{S}_{ij} = -2C_\tau \Delta k_{SGS}^{1/2} \bar{S}_{ij} \quad (3)$$

where, ν_{SGS} is the SGS turbulent viscosity. In this study, ν_{SGS} is modelled based on the localized dynamic k_{SGS} -equation model (LDKM) [12].

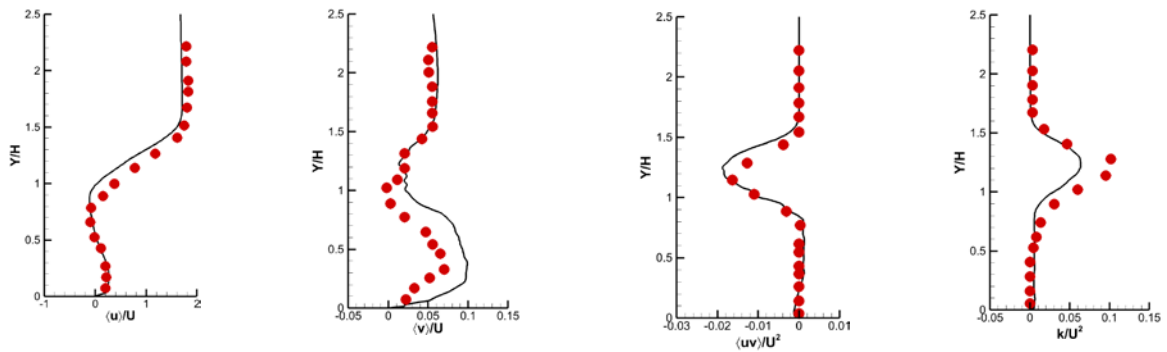
3.2. Numerical methods

The filtered governing equations are discretized by implementing the finite volume method. All the computations are carried out in the open-source object-oriented C^{++} programming in the OpenFOAM[13]. The second-order central difference scheme is adopted for spatial discretization, the implicit second-order backward difference scheme is used for the time integration, and the PISO algorithm is taken on for the pressure–velocity coupling in all the present simulations[14]. To accurately capture the evolution of the flow features the CFL number is kept below unity.

The computational domain is approximately discretized into 10.3 million non-uniform computational cells. For the evaluation of grid resolutions, two-point correlations are employed [15]. In this grid resolution assessment technique, the ratio of integral length scale (λ) to grid spacing is considered to be an appropriate method for the evaluation of grid resolution: The ratio demonstrates the number of cells in the resolved largest scale. In the present study, the ratio of integral length scale to the mean grid spacing for the streamwise (λ_{uu-Y}) and vertical (λ_{vv-Y}) integral length at the centre plane ($Z/D = 0$) at $X/D = 12$ is $\lambda_{uu-Y}/\bar{\Delta y} = 7.81$ and $\lambda_{vv-Y}/\bar{\Delta y} = 6.38$ in the vertical direction ($\bar{\Delta Y} = L_Y/N_Y$) respectively. Therefore, at least 6 cells have been included in the integral length scale that is sufficient [16].

3.3. Code validation

Before the LES study of partially filled channel flow, the solver has been validated based on laboratory experiments undertaken by Leu, et al. [17]. Fig. 3 compares the present LES results and experimental data for streamwise and vertical velocity components, Reynolds shear stress ($\langle u'v' \rangle$) and turbulent kinetic energy (TKE) above the porous block in the wake region at $X/H = 3$. The LES results show a good agreement with the reported data.



a) Streamwise velocity b) Vertical velocity c) Reynolds shear stress d) TKE
 Fig. 3 Comparison of vertical profiles of streamwise and vertical velocity, Reynold shear stress, $\langle u'v' \rangle / U^2$, and turbulent kinetic energy, $TKE = 0.5 (\overline{u'^2} + \overline{v'^2} + \overline{w'^2})$, against the experimental measurements of Leu, et al. [17] in the wake region at $X/H = 3$

4. Discussion of Results

4.1. Flow leakage

Fig. 4 shows contours of time-averaged vertical velocity on the crest and trough planes. The very first visible feature is that some portion of the fluid entering the porous blocks is pushed upwards to the porous-fluid interface and leaves the porous region halfway through to the clear region (flow leakage). This phenomenon is represented by the positive iso-surface of time-averaged vertical velocity in Fig. 5.

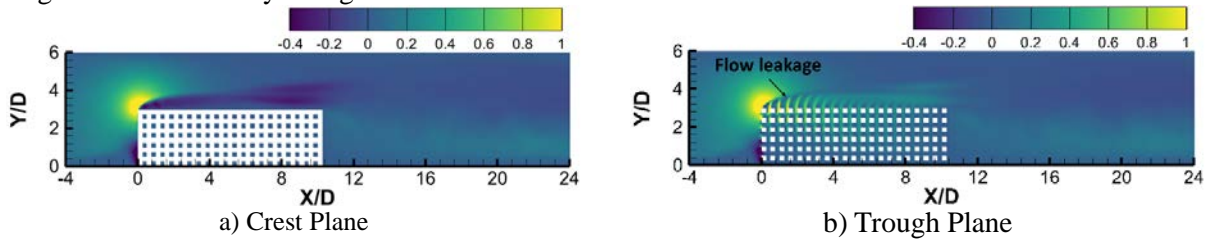


Fig. 4 Contours of time-averaged vertical velocity

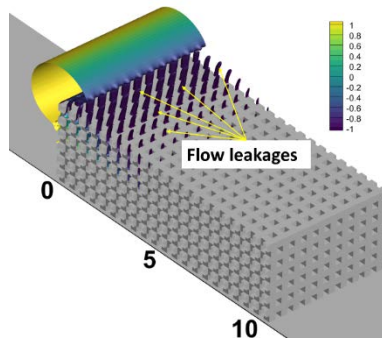


Fig. 5 Three-dimensional representation of the positive leakage from the porous block by iso-surface of vertical velocity ($\langle v \rangle / U = 0.5$) coloured by time-averaged pressure

Side view contours of the vertical velocity and streamlines in Fig. 6 demonstrate the upwards tendency of the flow that passes through the porous pores and penetrates the clear region across the interface.

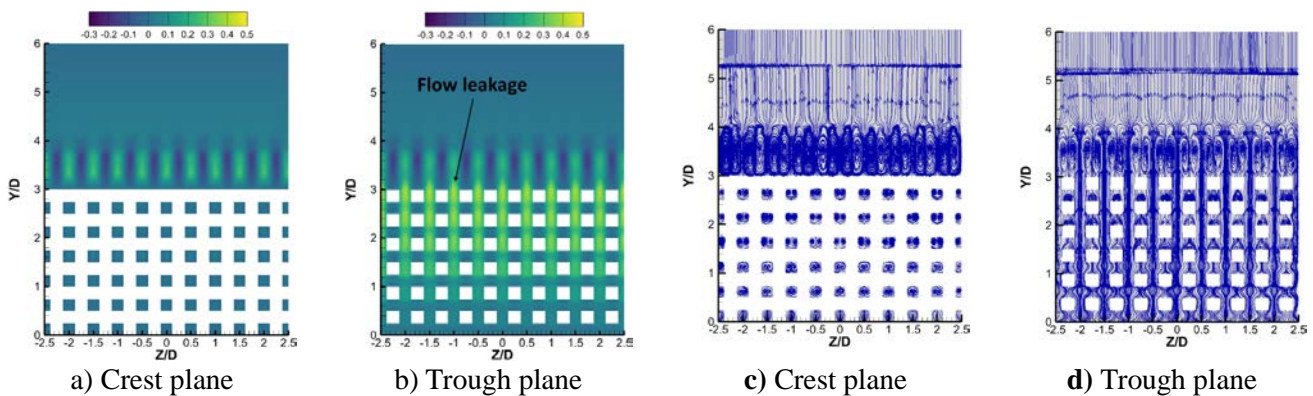


Fig. 6 Side view contours of vertical velocity and streamlines on crest and trough planes at $X/D = 4.5$; and $X/D = 5$ respectively

4.2. Porous and non-porous flow interaction

4.2.1. Spectral analysis in the porous region

Fig. 7 demonstrates the time history and power spectrum density (PDF) of vertical velocity at $Y/D = 1.38$ (almost in the middle height of the porous block) and different streamwise locations along the porous block. The periodic trend in the time history of vertical velocity in Fig. 7 (Left) demonstrates the presence of some dominant frequencies in the porous block.

Power spectral density plots of vertical velocity fluctuations are shown in Fig. 7 (Right). At $X/D = 1.38$ and 5.38 , two dominant frequencies appear initially at $f = 8.79$ and $f = 17.95$. However, as the flow develops ($X/D = 9.38$), energy is shifted to higher modes ($f = 17.95$). This observation shows the pulsating nature of the pore jet flow with dominant frequencies inside the porous blocks which is consistent with previous findings[18]. Blois, et al. [18] showed that the instantaneous structure within the pore space is dominated by jet flows. These jet flows could be horizontal, vertical or a combination of the two, with the temporal evolution of the pore flow being a function of the intensity, direction, and duration of these jets. They observed that flow characteristics in the pore space are caused by the pulsating nature of the pore jet flow.

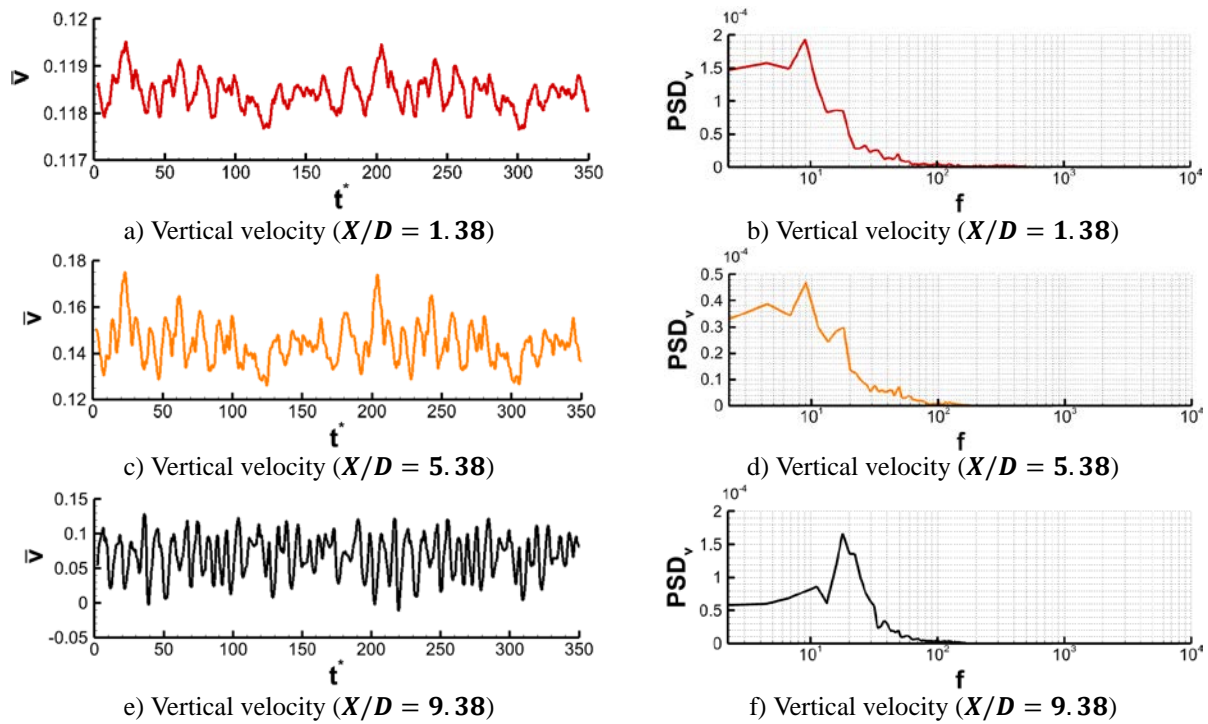


Fig. 7 Left: Time history and Right: Power spectrum density of streamwise and vertical velocity components within the porous block at $Y/D = 1.38$

4.2.2. Spectral analysis in the non-porous region

Fig. 8 depicts the time history and power spectrum density of the vertical velocity above the interface ($Y/D = 4$) at three streamwise locations, namely: near the beginning ($X/D = 1.38$); in the middle ($X/D = 5.38$), and near the ending ($X/D = 9.38$) of the porous block.

Above the interface near the beginning of the porous block ($X/D = 1.38$), velocity fluctuations reveal both low and high-frequency structures (Fig. 8 (a-b)). But, at $X/D = 5.38$, and $X/D = 9.38$ no low-frequency structures are observed. Comparison of Fig. 7 and Fig.8 shows that above the porous block, time histories are frequency-rich waveforms, whilst below the interface, they are simply a superposition of several sinusoidal waveforms.

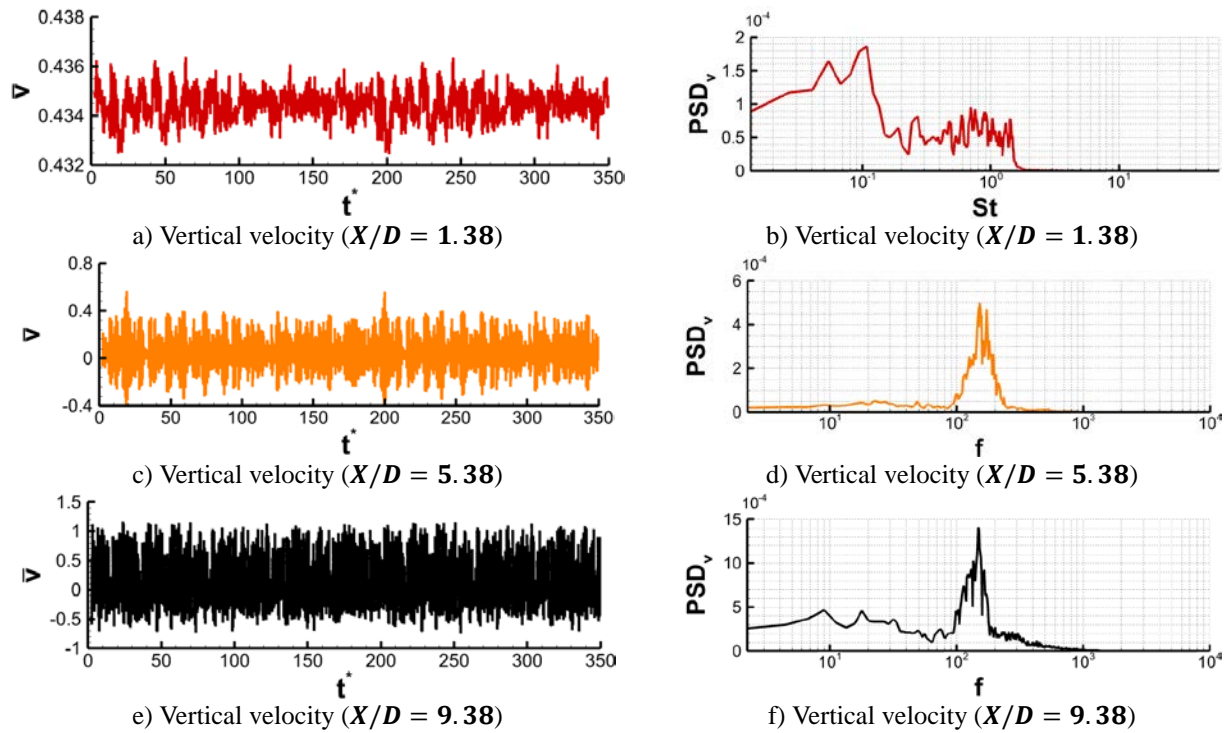


Fig. 8 Left: Time history and Right: Power spectrum density of vertical velocity above the porous block at $Y/D = 4$ on the trough plane at different streamwise locations

Table 1 lists the five strongest frequencies regarding Fig. 7 and Fig. 8. It shows that at the beginning of the porous block the two dominant frequencies (i.e., 8.97 and 17.95) within the porous block exist in the clear flow region. This observation confirms strong momentum transfer due to the flow leakage between the non-porous and porous flow.

At the middle ($X/D = 5.38$) and end ($X/D = 9.38$) of the porous block, the distribution of dominant frequencies is different from the beginning. For example, two dominant frequencies of 8.97 Hz and 17.54 Hz within the porous block are not observed in the top three strongest frequencies in the non-porous region. Because the vertical momentum of flow leakage at these regions are not strong enough to penetrate the shear layer.

Comparison of frequency content in the porous and non-porous regions in Table 1 shows that the high-frequency flow structures cannot advance deep inside the porous structures. For example, the following frequencies: $f = 116.6 \text{ Hz}$ and 125.6 Hz at $X/D = 1.38$; $f = 148 \text{ Hz}$ and 152.4 Hz at $X/D = 5.38$; $f = 148 \text{ Hz}$ at $X/D = 9.38$ are observed above the porous block, but cannot be found in the porous region. It means high-frequency flow structures are not capable to penetrate the porous block. In other words, the flow structures within the porous block are limited to the low-frequency flow structures.

Table 1 Strongest frequencies for streamwise and vertical velocity fluctuations at four streamwise locations along the porous block and five elevations within and above the porous block

		Vertical velocity fluctuation				
Frequency		f_1^{max}	f_2^{max}	f_3^{max}	f_4^{max}	f_5^{max}
Y/D	Streamwise position: At the begging of the porous block at X/D = 1.38					
0.12	Above bottom wall inside the porous block	49.37	-	-	-	-
1.62	In the middle height of porous block	8.97	17.94	49.35	-	-
2.62	Beneath the interface	8.97	17.94	33.65	49.37	42.63
3.2	Over the interface	8.97	17.94	116.6	33.65	42.63
4.0	At the shear layer above the interface	17.94	8.97	116.6	125.6	148
Y/D	Streamwise position: At the middle of the porous block at X/D=5.38					
0.12	Above bottom wall inside the porous block	49.37	-	-	-	-
1.62	In the middle height of porous block	8.97	17.94	49.37	-	-
2.62	Beneath the interface	8.97	17.94	22.44	26.92	49.37
3.2	Over the interface	8.97	17.94	22.44	49.37	148
4.0	At the shear layer above the interface	148	152.4	172.6	179.4	163.7
Y/D	Streamwise position: At the end of the porous block at X/D=9.38					
0.12	Above bottom wall inside the porous block	17.94	-	-	-	-
1.62	In the middle height of porous block	17.94	11.22	38.14	-	-
2.62	Beneath the interface	17.94	22.44	26.92	11.22	38.14
3.2	Over the interface	13.45	26.92	17.94	152.4	38.14
4.0	At the shear layer above the interface	148	136.8	165.9	130	123.3

4.2.3. Correlation between the porous and non-porous flow

Correlation coefficients of vertical velocity fluctuations are compared in Table 2 at three different regions, namely: within the porous block, across the interface, and above the porous block.

Below the interface, the magnitude of correlation coefficients reveals a strong positive correlation. This observation shows the upward tendency of flow inside the porous block demonstrated in Fig. 4. This trend is also observed across the interface that shows flow leakage across the interface connects porous flow to the non-porous flow.

At the beginning ($X/D = 0.38$) and end ($X/D = 9.88$) of the porous block, the correlation coefficients of vertical velocity fluctuations are anticorrelated; it is due to the flow reattachment near the leading edge of the porous block and the shear layer-wake interaction respectively.

Table 2 Correlation coefficients of vertical velocity fluctuations within, above and across the interface on the trough plane

Correlation coefficients within the porous block at two elevations: $Y_1/D = 1.63$ (In the middle height of the porous block) and $Y_2/D = 2.63$ (beneath the interface)												
X/D	0.38	0.88	1.38	2.38	3.38	4.38	5.38	6.38	7.38	8.38	9.38	9.88
$\rho(v'_{Y1}, v'_{Y2})$	0.75	0.85	0.73	0.96	0.93	0.68	0.93	0.93	0.94	0.89	0.82	0.74
Correlation coefficients across the porous block interface at two elevations: $Y_2/D = 2.63$ (beneath the interface) and $Y_3/D = 3.2$ (over the interface)												
X/D	0.38	0.88	1.38	2.38	3.38	4.38	5.38	6.38	7.38	8.38	9.38	9.88
$\rho(v'_{Y2}, v'_{Y3})$	-0.16	0.55	0.83	0.83	0.75	0.63	0.76	0.77	0.77	0.54	0.10	-0.01
Correlation coefficients above the porous block at two elevations $Y_3/D = 3.2$ (over the interface) and $Y_4/D = 4$ (above the interface at the shear layer)												
X/D	0.38	0.88	1.38	2.38	3.38	4.38	5.38	6.38	7.38	8.38	9.38	9.88
$\rho(v'_{Y3}, v'_{Y4})$	-0.09	-0.07	-0.07	0.04	0.22	0.26	0.30	0.31	0.26	0.28	0.24	0.26

5. Conclusions

The main findings are summarised as follows:

1. Flow visualization reveals that some portion of the fluid entering the porous blocks is pushed upwards into the porous-fluid interface and leaves the porous region halfway through to the clear region (flow leakage).
2. Correlation coefficients show an interaction between porous and non-porous flow due to flow leakage. Below the interface, the magnitude of correlation coefficients indicates a strong positive correlation between vertical velocity fluctuations that reinforces the idea of the upward tendency of flow inside the porous block. This tendency is also observed across the interface which confirms the momentum transfer through the interface.
3. Above the porous block interface, PDF of velocity components demonstrate frequency-rich waveforms whilst below the interface, velocity components are simply a superposition of several sinusoidal waveforms.
4. Comparison of frequency content in the porous and non-porous region shows the high-frequency flow structures are not capable to penetrate the porous block. In other words, the flow structures within the porous region are limited to the low-frequency flow structures.
5. The frequency content of vertical velocity in the porous and non-porous region demonstrates that the two first dominant frequencies in the porous region exist in the non-porous region. This observation confirms strong momentum transfer due to the flow leakage between the porous and non-porous region, where the flow leakage is pronounced.

6. Acknowledgements

This work was supported by the UK Engineering and Physical Sciences Research Council (EPSRC) [grant numbers EP/T012242/1 and EP/T012242/2]. Data supporting this publication can be obtained on request. The authors would like to acknowledge the assistance given by Research IT and the use of the Computational Shared Facility at The University of Manchester.

Reference

- [1] X. Chu, W. Wang, G. Yang, A. Terzis, R. Helmig, and B. Weigand, "Transport of Turbulence Across Permeable Interface in a Turbulent Channel Flow: Interface-Resolved Direct Numerical Simulation," *Transport in Porous Media*, vol. 136, no. 1, pp. 165-189, 2021-01-01 2021, doi: [10.1007/s11242-020-01506-w](https://doi.org/10.1007/s11242-020-01506-w).
- [2] Y. Kuwata and K. Suga, "Transport Mechanism of Interface Turbulence over Porous and Rough Walls," *Flow, turbulence and combustion*, vol. 97, no. 4, pp. 1071-1093, 2016, doi: [10.1007/s10494-016-9759-9](https://doi.org/10.1007/s10494-016-9759-9).
- [3] A. Leonardi, D. Pokrajac, F. Roman, F. Zanello, and V. Armenio, "Surface and subsurface contributions to the build-up of forces on bed particles," *J. Fluid Mech.*, vol. 851, pp. 558-572, 2018-09-25 2018, doi: [10.1017/jfm.2018.522](https://doi.org/10.1017/jfm.2018.522).
- [4] T. Poulsen and Y. Yuan, "Predicting below-surface horizontal pore gas velocity in porous media from above-surface wind conditions and medium gas permeability," *European journal of soil science*, vol. 72, no. 1, pp. 183-197, 2021, doi: [10.1111/ejss.12983](https://doi.org/10.1111/ejss.12983).
- [5] W. Wang, X. Chu, A. Lozano-Durán, R. Helmig, and B. Weigand, "Information transfer between turbulent boundary layers and porous media," *J. Fluid Mech.*, vol. 920, 2021, doi: [10.1017/jfm.2021.445](https://doi.org/10.1017/jfm.2021.445).
- [6] F. Shikh Anuar, K. Hooman, M. R. Malayeri, and I. Ashtiani Abdi, "Experimental study of particulate fouling in partially filled channel with open-cell metal foam," *Experimental Thermal and Fluid Science*, vol. 110, p. 109941, 2020/01/01/ 2020, doi: <https://doi.org/10.1016/j.expthermflusci.2019.109941>.
- [7] F. Shikh Anuar, I. Ashtiani Abdi, and K. Hooman, "Flow visualization study of partially filled channel with aluminium foam block," *International Journal of Heat and Mass Transfer*, vol. 127, pp. 1197-1211, 2018-12-01 2018, doi: [10.1016/j.ijheatmasstransfer.2018.07.047](https://doi.org/10.1016/j.ijheatmasstransfer.2018.07.047).
- [8] M. Jadidi, A. Revel, and Y. Mahmoudi, "Pore scale large eddy simulation of flow in a channel partially filled with porous block," in *15th International Conference on Heat Transfer, Fluid Mechanics and Thermodynamics (ATE-HEFAT2021)*, Virtual Conference, 26-28 July 2021: HEFTA, 2021, pp. 1839-1844.

- [9] B. Alazmi and K. Vafai, "Analysis of fluid flow and heat transfer interfacial conditions between a porous medium and a fluid layer," *International Journal of Heat and Mass Transfer*, vol. 44, no. 9, pp. 1735-1749, 2001/05/01/ 2001, doi: [https://doi.org/10.1016/S0017-9310\(00\)00217-9](https://doi.org/10.1016/S0017-9310(00)00217-9).
- [10] M. J. S. De Lemos, "Turbulent Flow Around Fluid–Porous Interfaces Computed with a Diffusion-Jump Model for k and ε Transport Equations," *Transport in Porous Media*, vol. 78, no. 3, pp. 331-346, 2009, doi: [10.1007/s11242-009-9379-0](https://doi.org/10.1007/s11242-009-9379-0).
- [11] S. B. Pope, *Turbulent Flows*. Cambridge: Cambridge University Press, 2000.
- [12] W.-W. Kim and S. Menon, "Application of the localized dynamic subgrid-scale model to turbulent wall-bounded flows," in *35th aerospace sciences meeting and exhibit*, 1997, p. 210.
- [13] H. Jasak, A. Jemcov, and Z. Tukovic, "OpenFOAM: A C++ library for complex physics simulations," in *International workshop on coupled methods in numerical dynamics*, 2007, vol. 1000: IUC Dubrovnik Croatia, pp. 1-20.
- [14] H. K. Versteeg and W. Malalasekera, *An introduction to computational fluid dynamics: the finite volume method*, 2nd ed. ed. Harlow, England;: Pearson Education Ltd., 2007.
- [15] F. Bazdidi-Tehrani, A. Ghafouri, and M. Jadidi, "Grid resolution assessment in large eddy simulation of dispersion around an isolated cubic building," *Journal of Wind Engineering and Industrial Aerodynamics*, vol. 121, pp. 1-15, 2013/10/01/ 2013, doi: <https://doi.org/10.1016/j.jweia.2013.07.003>.
- [16] L. Davidson, "How to estimate the resolution of an LES of recirculating flow," in *Quality and Reliability of Large-Eddy Simulations II*: Springer Netherlands, 2011, pp. 269-286.
- [17] J. M. Leu, H. C. Chan, and M. S. Chu, "Comparison of turbulent flow over solid and porous structures mounted on the bottom of a rectangular channel," *Flow Measurement and Instrumentation*, vol. 19, no. 6, pp. 331-337, 2008/12/01/ 2008, doi: <https://doi.org/10.1016/j.flowmeasinst.2008.05.001>.
- [18] G. Blois, G. H. Sambrook Smith, J. L. Best, R. J. Hardy, and J. R. Lead, "Quantifying the dynamics of flow within a permeable bed using time-resolved endoscopic particle imaging velocimetry (EPIV)," *Experiments in Fluids*, vol. 53, no. 1, pp. 51-76, 2012/07/01 2012, doi: [10.1007/s00348-011-1198-8](https://doi.org/10.1007/s00348-011-1198-8).